3rd URSI AT-AP-RASC, Gran Canaria, 29 May – 3 June 2022

Finite Element-Boundary Integral Simulation of Icing Effects on a Marine Radar Reflector

Niklas Wingren*(1) and Daniel Sjöberg(1)
(1) Lund University, Lund, Sweden

Abstract

This paper presents simulations of the radar cross section for a marine corner reflector affected by icing as it is illuminated by 3 GHz marine radar. This is compared to the radar cross section for an unaffected reflector, and the consequences for radar range are investigated. To perform the simulations, a finite element-boundary integral hybrid method is used. The simulation code is based on several open-source packages, of which the most important are FEniCSx and Bempp-cl. Simulations show a large reduction in maximum radar range due to icing, with a maximum reduction by 60 % found near boresight.

1 Introduction

Radar reflectors are widely used in marine settings to enhance radar visibility of targets such as smaller vessels and buoys. This is one tool to avoid collisions with larger vessels as they are required to have a radar fitted at either 9 GHz or both 3 GHz and 9 GHz, depending on their gross tonnage [1]. If a reflector is to be relied upon, its radar cross section (RCS) must be sufficiently large so that other vessels can detect it early enough to take action. Due to this, it can be interesting to evaluate the performance of a reflector under various conditions it may experience.

One way to evaluate electromagnetic performance is to perform measurements. However, these can be expensive, which is why it is nowadays common to first use numerical simulations. Many different numerical methods are available, and they are suitable to different types of problems. The method of moments (MoM) is often used for scattering problems, but it has difficulties with problems involving inhomogeneous materials. The finite element method (FEM) is commonly used for problems involving such materials, but is not optimal for use for problems containing large regions of free space. The finite element-boundary integral (FE-BI) method is a hybrid method aiming at combining the best properties of FEM and MoM by terminating a FEM mesh by a MoM boundary [2].

In this work we investigate the effect of icing on the RCS of a marine corner reflector. As such a reflector contains a large free-space region within it, and as different types of ice can be involved, we use a FE-BI method. The method is implemented in Python using open-source packages.

2 FE-BI Formulation and Implementation

The formulation in this work is similar to that presented in chapter 11.8.1 of [2], but uses the electric field integral equation (EFIE) instead of the combined field integral equation and handles degrees of freedom (DoFs) slightly differently. The FE-BI system in our modified formulation is

$$\begin{bmatrix} K & T^{\mathrm{IS}}B \\ P^{\mathrm{E}}T^{\mathrm{SI}} & Q^{\mathrm{E}} \end{bmatrix} \begin{Bmatrix} E \\ \bar{H}^{\mathrm{S}} \end{Bmatrix} = \begin{Bmatrix} b \\ b^{\mathrm{E,inc}} \end{Bmatrix}. \tag{1}$$

K is the FE system matrix equivalent to the combination of all K^{XY} blocks in [2], but not necessarily structured the same. B comes from enforcing Maxwell's equations on the surface and is the same as in [2]. E and $\bar{H}$ are vectors for electric field and surface magnetic field DoFs. b and $b^{\mathrm{E,inc}}$ are source vectors corresponding to interior currents and incident electric fields. T^{SI} and T^{IS} map from all DoFs to those on the surface and vice versa, and are used instead of explicitly separating interior and surface DoFs in blocks. P^{E} and Q^{E} are from the EFIE and can be written

$$P^{\mathrm{E}}_{ij} = \oint_{S_0} \boldsymbol{t}_i(\boldsymbol{r}) \cdot \left[\frac{1}{2}\boldsymbol{\Lambda}_j + \hat{\boldsymbol{n}} \times \tilde{\mathscr{K}}(\boldsymbol{\Lambda}_j) \right] \mathrm{d}S \tag{2}$$

$$Q^{\mathrm{E}}_{ij} = \oint_{S_0} \boldsymbol{t}_i(\boldsymbol{r}) \cdot [\hat{\boldsymbol{n}} \times \mathscr{L}(\boldsymbol{\Lambda}_j)] \, \mathrm{d}S \tag{3}$$

where S_0 is the outer boundary, $\tilde{\mathscr{K}}$ and $\mathscr{L}$ are the same integral operators as in [2], $\boldsymbol{\Lambda}_j$ are Rao-Wilton-Glisson basis functions and $\boldsymbol{t}_i$ are scaled Nédélec testing functions.

In the solution of the system we use an inward-looking approach, i.e. eliminating the interior DoFs using the upper row of (1). In the absence of interior current sources b, the system can be written on the form

$$KX = T^{\mathrm{IS}}B \tag{4}$$

$$\left(Q^{\mathrm{E}} - P^{\mathrm{E}}T^{\mathrm{SI}}X\right)\bar{H}^{\mathrm{S}} = b^{\mathrm{E,inc}} \tag{5}$$

$$E = -X\bar{H}^{\mathrm{S}}. \tag{6}$$

By solving for X, $\bar{H}^{\mathrm{S}}$ and E in sequence, the same solution is obtained. Due to the nature of FE matrices, K and $T^{\mathrm{IS}}B$ can be stored in a sparse format. The intermediate solution X is not sparse though, which must be taken into account in the solution process. The BI matrices are dense, so the system matrix in (5) is dense. Since some matrices can be stored in a sparse format, this approach can be advantageous for direct solvers when compared to solving (1) with the system matrix in a dense format.

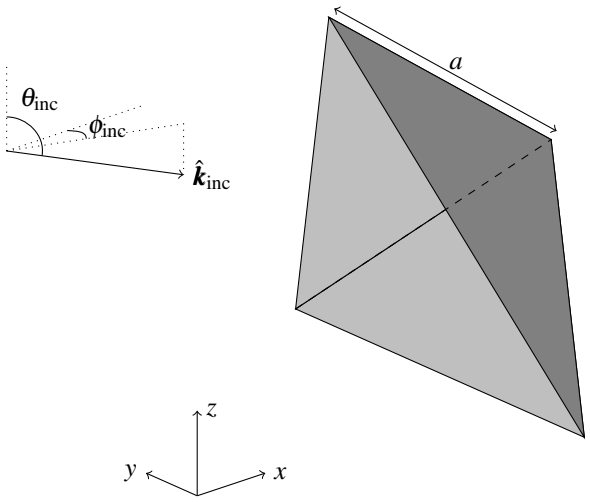

Figure 1. Corner reflector with incident wave.

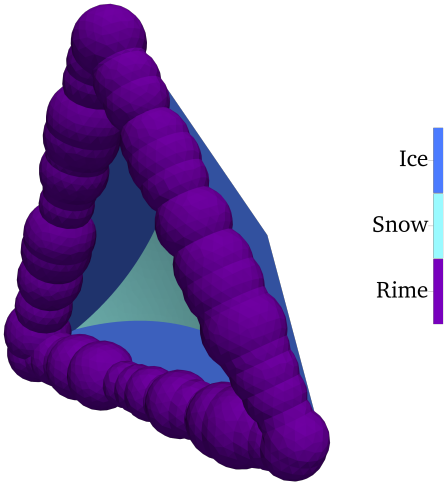

Figure 2. Reflector with icing.

To implement the FE-BI code, we used several open-source packages. FEniCSx, which is the development version of the FEniCS project [3], [4] consisting of DOLFINx [5], FFCx [6], Basix [7] and UFL [8], [9], was used to implement FE operators. Bempp-cl [10], [11] was used to implement BI operators, including a coupling to FEniCSx. Gmsh [12] was used to generate geometries and meshes which were imported to FEniCSx using the file `gmsh_helpers.py` from [13]. After all operators were set up and assembled, the solution was computed using a combination of direct solvers from SciPy [14]. The FE-BI code was tested for the problem of scattering against a PEC sphere layered with a lossy dielectric and the solution was compared to an analytical Mie solution. Good agreement was observed, and the numerical solution could be seen to converge to the analytical with a decrease in mesh size.

3 Corner Reflector Example

To demonstrate a realistic use case for the FE-BI code, we investigated the effect of icing on the monostatic RCS of a marine corner reflector. A sketch of the problem is shown in figure 1 where a trihedral corner reflector is illuminated by a plane wave traveling in the direction of $\hat{\boldsymbol{k}}_{\text{inc}}$. The reflector is oriented such that the bottom surface is angled at 35° to the sea surface (the xy-plane in the figure). The sea surface itself was not included in the model. This configuration can be seen in clusters of trihedral corner reflectors mounted on buoys [1]. The problem was considered for radar at 3 GHz due to its lower attenuation from weather like snow, fog and rain compared to 9 GHz [15]. All these conditions can cause icing [16], which is the effect of interest here. Simulations were performed for a reflector with $a = 20$ cm, corresponding to $2\lambda_0$ at 3 GHz. Two cases were considered: a reflector unaffected and affected by icing.

In the first case, the reflector was composed of three triangular PEC sheets with a thickness of 3 mm. The corners by the opening of the reflector were truncated. The surface of the reflector was meshed into triangles using Gmsh with element size $\lambda_0/10$. Bempp-cl was used to set up and solve the EFIE for incident plane waves, and the monostatic RCS was computed using far field operators from Bempp-cl.

In the second case, the previously described geometry was modified to add icing. A 3 mm layer of impure ice was added to the reflector surfaces. Rime ice was added to the edges with some irregularity by joining solid spheres of different sizes. Accumulated snow was added inside the reflector. The geometry with icing is shown in figure 2. The different dielectric properties are listed in table 1, where $\varepsilon_{\text{r}} = \varepsilon_{\text{r}}' + \mathrm{i}\varepsilon_{\text{r}}''$ and $\mu_{\text{r}} = 1$ for all materials. For ice, the measured properties for freshwater ice with salt impurities at -5°C and 3.7 GHz were used [17]. For snow and rime, the empirical model for dry snow from [18] was used at -5°C and 3 GHz. The snow density was in the lower range of wind-affected dry snow at 300 kg/m^3 [19], and the rime density was that of hard rime at 700 kg/m^3 [16].

Table 1. Material parameters.

Material	ε_{r}'	ε_{r}''
Ice	3.18	0.0015
Snow	1.6	0.000288
Rime	2.4	0.000846

The combined volume of ice, snow and rime was meshed into tetrahedrals in Gmsh with element sizes $\lambda_0/(10\sqrt{\varepsilon_{\text{r}}'})$. The operators for the FE-BI formulation were set up using FEniCSx and Bempp-cl, where a PEC boundary condition was used at the interior boundary of the reflector surface. Using these operators, the FE-BI system was solved using the inward-looking approach described in (4)–(6). The solutions for multiple incident plane waves (corresponding to multiple $b^{\text{E,inc}}$) were computed in a relatively efficient way by reusing the same X from (4) and the same LU-factorization for each solution of (5). As in the PEC case, the monostatic RCS was computed using far field operators from Bempp-cl.

The two cases were simulated for horizontally polarized incident plane waves with propagation directions in the range $\theta_{\text{inc}} \in [50^\circ, 170^\circ]$ and $\phi_{\text{inc}} \in [-60^\circ, 60^\circ]$. Horizontal polarization was selected as that is the most common for marine radar [1]. Simulations were also performed with a denser spacing in ϕ_{inc} where $\theta_{\text{inc}} = 90^\circ$ was fixed, corresponding to radar positions far from the reflector. These are interesting as that is where the reflector would first be detected.

4 Simulation Results and Discussion

Figure 3 shows the monostatic RCS for the two cases with incident plane waves having propagation directions $(\phi_{\text{inc}}, \theta_{\text{inc}})$. By comparing the two figures, it can be seen that the reflector affected by icing is effective across less of the angular range. The large reduction in RCS around $(\phi_{\text{inc}}, \theta_{\text{inc}}) = (0^\circ, 90^\circ)$ in figure (b) is also interesting to note since this is a region where one would like a reflector to work well. A property of the trihedral reflector which also is seen in the RCS pattern of figure (a) is the symmetry about the xz-plane ($\phi_{\text{inc}} = 0$ in the figure). This symmetry is not preserved in figure (b), which makes sense as the rime layer is asymmetric.

Figure 4 shows the monostatic RCS for the two cases, but with incident waves along the *xy*-plane. It can be seen that the reflector affected by icing only has two narrow lobes where the RCS performance is similar to that of the unaffected reflector. These lobes are located near the edges of where a trihedral is commonly deemed effective ($\pm 22^\circ$ by [1]). The largest difference between the lines in figure 4 is found at -6° where there is a 16 dB reduction in RCS due to icing. However, the reduction is large in the entire range between -10° and 10°.

The effect of icing on general radar performance can be evaluated using the radar range equation, but if only RCS is changed it is sufficient to use the relation $R \sim \sigma^{1/4}$ for the maximum range R and RCS σ [15]. This holds if atmospheric attenuation is disregarded, which can be reasonable in, for example, foggy conditions below 5 GHz as the attenuation coefficient is then mostly negligible [15]. For comparison, typical one-way attenuation coefficients at 10 GHz for those conditions are between $0.02 - 3$ dB/km [15]. The reduction in RCS by 16 dB which was found at $\phi_{\text{inc}} = -6^\circ$ thus corresponds to a reduction in maximum range by 60 %. A more modest 10 dB reduction would still correspond to a 44 % reduction in maximum range.

5 Conclusion

A FE-BI code for electromagnetic computations has been presented as applied to the problem of icing on a marine corner reflector. The results of simulating a corner reflector with and without icing have shown that icing can have a significant effect on the monostatic RCS of such a reflector. Furthermore, this has been related to the maximum range for detection by a 3 GHz radar.

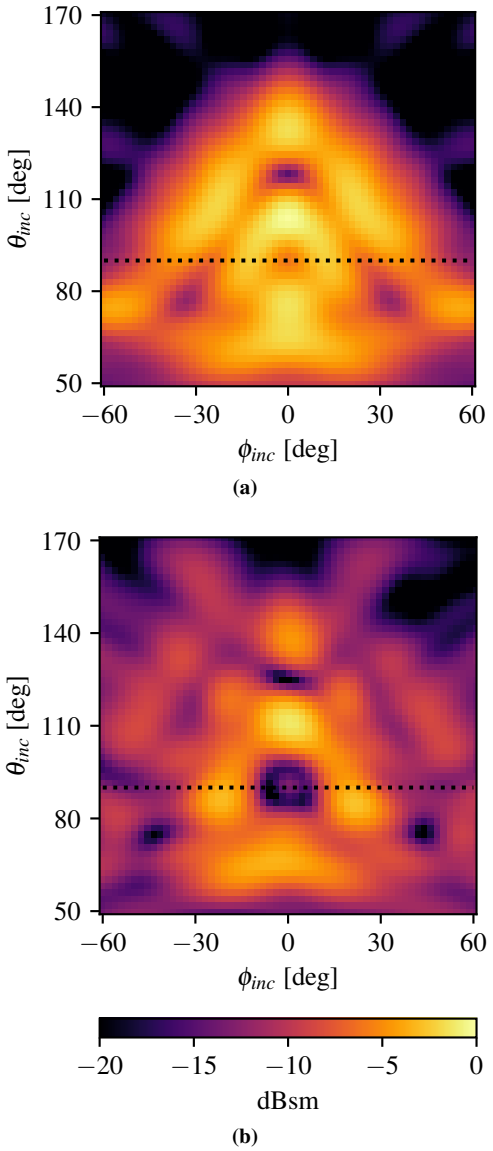

Figure 3. Monostatic RCS for reflector. (a) Unaffected by icing. (b) Affected by icing. *xy*-plane marked by dashed line.

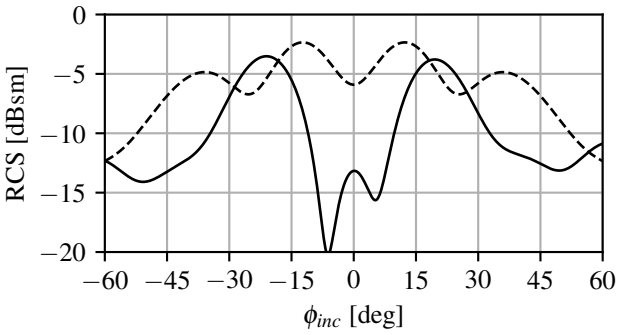

Figure 4. Monostatic RCS in *xy*-plane for reflector unaffected (dashed) and affected (solid) by icing.

The results indicate that a corner reflector exposed to icing weather conditions could be at risk of significant performance degradation. However, this work only considered a single, fairly small reflector and with only one icing configuration. A reason for the small physical size is memory limitations due to the use of direct solvers in the code. Although the inward-looking approach in (4)–(6) was more memory-efficient than a direct solution of (1), it still required dense storage of the intermediate matrix X. One possible improvement would be to solve (1) iteratively since sparse and dense matrix blocks can then be stored as such. This would require an appropriate preconditioner to be effective. Further improvements could include acceleration methods for the BI part since its corresponding matrix blocks are dense.

6 Acknowledgements

This work was supported in part by the Swedish Armed Forces, in part by the Swedish Defence Materiel Administration, in part by the National Aeronautics Research Program and in part by the Swedish Governmental Agency for Innovation Systems. We would also like to thank Tomas Lundin for valuable discussions.

References

[1] J. N. Briggs, *Target Detection by Marine Radar*, ser. Radar, Sonar &; Navigation. London, U.K.: Institution of Engineering and Technology, 2004.

[2] J.-M. Jin, *Theory and Computation of Electromagnetic Fields*. Hoboken, NJ, USA: John Wiley & Sons, Ltd, 2010.

[3] M. Alnæs, J. Blechta, J. Hake, *et al.*, "The FEniCS project version 1.5," *Archive of Numerical Software*, vol. 3, no. 100, 2015.

[4] A. Logg, K.-A. Mardal, and G. Wells, *Automated solution of differential equations by the finite element method: The FEniCS book*. Berlin, Germany: Springer Science & Business Media, 2012.

[5] G. N. Wells, F. Ballarin, I. A. Baratta, *et al.* "DOLFINx: Next generation FEniCS problem solving environment." (2021), [Online]. Available: `https://github.com/FEniCS/dolfinx` (visited on Jan. 5, 2022).

[6] G. N. Wells, I. A. Baratta, M. Habera, J. S. Hale, C. N. Richardson, and M. W. Scroggs. "FFCx: Next generation FEniCS form compiler." (2021), [Online]. Available: `https://github.com/FEniCS/ffcx` (visited on Jan. 5, 2022).

[7] C. Richardson, M. Scroggs, and G. Wells. "Basix: FEniCS finite element basis evaluation library." (2021), [Online]. Available: `https://github.com/FEniCS/basix` (visited on Jan. 5, 2022).

[8] M. S. Alnæs, A. Logg, K. B. Ølgaard, M. E. Rognes, and G. N. Wells, "Unified form language: A domain-specific language for weak formulations of partial differential equations," *ACM Trans. Math. Softw.*, vol. 40, no. 2, 2014.

[9] M. S. Alnaes, "Ufl: A finite element form language," in *Automated Solution of Differential Equations by the Finite Element Method*, A. Logg, K.-A. Mardal, and G. Wells, Eds. Springer Science & Business Media, 2012.

[10] T. Betcke and M. W. Scroggs, "Bempp-cl: A fast python based just-in-time compiling boundary element library.," *Journal of Open Source Software*, vol. 6, no. 59, p. 2879, 2021.

[11] M. W. Scroggs, T. Betcke, E. Burman, W. Śmigaj, and E. van 't Wout, "Software frameworks for integral equations in electromagnetic scattering based on calderón identities," *Computers & Mathematics with Applications*, vol. 74, no. 11, pp. 2897–2914, 2017.

[12] C. Geuzaine and J.-F. Remacle, "Gmsh: A 3-D finite element mesh generator with built-in pre-and post-processing facilities," *International journal for numerical methods in engineering*, vol. 79, no. 11, pp. 1309–1331, 2009.

[13] J. S. Dokken, *Using the GMSH Python API to generate complex meshes*. [Online]. Available: `http://jsdokken.com/converted_files/tutorial_gmsh.html` (visited on Jan. 10, 2022).

[14] P. Virtanen, R. Gommers, T. E. Oliphant, *et al.*, "SciPy 1.0: Fundamental Algorithms for Scientific Computing in Python," *Nature Methods*, vol. 17, pp. 261–272, 2020.

[15] M. A. Richards, J. A. Scheer, and W. A. Holm, Eds., *Principles Of Modern Radar*. Raleigh, NC, USA: SciTech Publishing, Inc., 2010, vol. 1: Basic Principles.

[16] S. Fikke, G. Ronsten, A. Heimo, *et al.*, "COST 727: Atmospheric icing on structures: Measurements and data collection on icing: State of the art," Publication of MeteoSwiss, 75, 2006, pp. 13–16.

[17] C. Matzler and U. Wegmuller, "Dielectric properties of freshwater ice at microwave frequencies," *Journal of Physics D: Applied Physics*, vol. 20, no. 12, pp. 1623–1630, Dec. 1987.

[18] M. Tiuri, A. Sihvola, E. Nyfors, and M. Hallikaiken, "The complex dielectric constant of snow at microwave frequencies," *IEEE Journal of Oceanic Engineering*, vol. 9, no. 5, pp. 377–382, 1984.

[19] J. Pomeroy and E. Brun, "Physical properties of snow," in *Snow ecology: an interdisciplinary examination of snow-covered ecosystems*, H. G. Jones, J. W. Pomeroy, D. A. Walker, and R. W. Hoham, Eds. Cambridge, U.K.: Cambridge University Presss, 2001, p. 101.